Valence photoelectron spectra of alkali bromides calculated within the propagator theory

Karpenko, Alexander; Iablonskyi, Denys; Aksela, Helena

Published in:
Journal of Chemical Physics

Link to article, DOI:
10.1063/1.4802054

Publication date:
2013

Document Version
Publisher's PDF, also known as Version of record

Valence photoelectron spectra of alkali bromides calculated within the propagator theory

Alexander Karpenko, Denys Iablonskyi, and Helena Aksela

Citation: J. Chem. Phys. **138**, 164315 (2013); doi: 10.1063/1.4802054
View online: http://dx.doi.org/10.1063/1.4802054
View Table of Contents: http://jcp.aip.org/resource/1/JCPSA6/v138/i16
Published by the American Institute of Physics.

Valence photoelectron spectra of alkali bromides calculated within the propagator theory

Alexander Karpenko,[1,2,a)] Denys Iablonskyi,[1] and Helena Aksela[1]
[1]*Department of Physical Sciences, University of Oulu, P.O. Box 3000, Fin-90014 Oulu, Finland*
[2]*Center for Atomic-Scale Materials Design (CAMD), Department of Physics, Technical University of Denmark, Building 307, DK-2800 Kgs. Lyngby, Denmark*

(Received 19 December 2012; accepted 3 April 2013; published online 25 April 2013)

The valence ionization spectra covering the binding energy range 0–45 eV of alkali bromide XBr (X = Li, Na, K, Rb) vapors are studied within the framework of the propagator theory. Relativistic Algebraic Diagrammatic Construction calculations have been carried out in order to investigate photoionization processes and to describe molecular electronic structure. Theoretical results are compared with available experimental data. © *2013 AIP Publishing LLC*. [http://dx.doi.org/10.1063/1.4802054]

I. INTRODUCTION

Ionization processes of alkali halide vapors have been studied by photoelectron (PE) spectroscopy technique for the last four decades.[1,2] The technique gives information about electronic structure and provides chemical characterization of alkali halide microclusters.[3] The valence PE spectra of alkali halides have been recorded earlier, with HeI, HeII discharge lamp excitation.[4–6] During the last decade the use of synchrotron radiation (SR) as an exciting source has become a standard technique in electron spectroscopy of alkali halide vapors.[7–9]

Nowadays, computational methods have become an important approach to understand chemical bonds of molecular systems, as well as to help in interpretation of experimental PE spectra. Accurate calculation of PE spectra of alkali halides, containing heavy elements (Br and Rb) with significant spin-orbit splitting and electron correlation, is a challenging task. The relativistic methods are a natural way of treating such systems.

Tomasello *et al*. investigated the vertical valence ionization potentials of the $(NaCl)_2$ dimer by means of two all-electron *ab initio* self-consistent field-HF (SCF-HF) based Green's function (GF) methods.[10]

More recently, Pernpointner *et al*.[11] carried out calculations of alkali iodide valence PE spectra in order to reproduce experimental valence ionization spectra. Fully relativistic calculations for the ionization spectra of hydrogen iodide (HI) and alkali iodides MI (M = Li, Na, K, Rb) were carried out using a one-particle propagator technique in a four-component framework. Pernpointner *et al*.[12] investigated by means of relativistic computations of ionization spectra of small $(HI)_2$, $(LiI)_2$ clusters, and subsequent electronic decay of cations.

In this work, we investigated valence photoelectron spectra of alkali bromides. By using the third-order algebraic diagrammatic construction (ADC(3)) method we calculated the binding energies and ionization strengths for 4*p* and 4*s* orbitals of Br^-, 3*p* and 3*s* orbitals of K^+, 2*p* orbital of Na^+, and 4*p* and 4*s* orbitals of Rb^+. For KBr this is a continuation of an earlier study by Caló *et al*.,[9] who performed calculations based on configuration interaction (CI) and multiconfigurational self-consistent field (MCSCF) methods for ionization energies.

For KBr, we found theoretical ionization energies to be in close agreement with experimental data[9] taken using synchrotron radiation source. ADC(3) calculations for LiBr, NaBr, and RbBr are expected to be similarly accurate and may support future experiments. To the best of our knowledge no experimental inner-valence ionization spectra of these molecules are available so far.

II. THEORY AND COMPUTATIONS

Green's function methods represent a very useful tool for calculation of the electron ionization potentials, electron affinities, excitation energies, and other properties. In the literature there are two major Green's function approaches to investigate the ionization process: an outer-valence Green's function (OVGF) approximation[13,14] and second- or third-order algebraic diagrammatic construction.[15] The overview of Green's function methods can be found in Ref. 16.

ADC is an approximation scheme which is the most practical and systematic for Green's function evaluation. The problem of finding the pole positions and pole strengths of a Green's function is formulated in terms of the solution of a matrix eigenvalue problem. Originally, the method was formulated by J. Schirmer.[15] A more detailed discussion of the ADC scheme can be found in Refs. 17 and 18.

Spectral intensities, which are measured in the photoelectron experiment are related to transition probability amplitudes. They are related to the one particle Green's function. In energy representation GF can be expressed in the form of spectral representation

$$G_{pq}(\omega) = G^{+}_{pq}(\omega) + G^{-}_{pq}(\omega), \tag{1}$$

where $G^{+}_{pq}(\omega)$, $G^{-}_{pq}(\omega)$ represent information about $(N \pm 1)$-particle systems, respectively. $(N - 1)$ particle part

a)Electronic mail: oleksandr.karpenko@oulu.fi

corresponds to singly ionized system and can be written in the form

$$G^{-}_{pq}(\omega) = \sum_{n} \frac{x^{*}_{nq} x_{np}}{\omega - \omega_n - i\eta}, \tag{2}$$

where the poles ω_n,

$$\omega_n = -\left(E^{N-1}_{n} - E^{N}_{0}\right), \tag{3}$$

are the nth ionization energies of the system and x_{np} are the transition probability amplitudes

$$x_{np} = \left\langle \Psi^{N-1}_{n} \middle| c_p \middle| \Psi^{N}_{0} \right\rangle. \tag{4}$$

The simplest form of the (relative) photoelectron spectral intensities P_n can be evaluated as

$$P_n \sim \sum_{p} \left| x^{(n)}_{p} \right|^2. \tag{5}$$

All calculations have been performed using the fully relativistic one-particle propagator framework RELADC[19,20] implemented in DIRAC10.[21] The calculations for molecules have been carried out in C_{2v} double-group symmetry. The spin-orbit coupling was discernible directly from the relativistic treatment.

The molecular bond lengths were taken from the experimental data, 2.17 Å[22] for LiBr, 2.50 Å[23] for NaBr, 2.915 Å[9] for KBr, and 2.94 Å[24] for RbBr.

For calculations of lithium, sodium, and potassium the 6-311++G(2d,2p) basis set[25–27] has been used from the DIRAC10 basis library. Bromine and rubidium have been studied using the valence quadruple-zeta dyall.av4z basis set being developed by Ken Dyall.[28] Four-component Dirac-Coulomb Hamiltonian was chosen for all ADC(3) calculations. Gaunt corrections were included for self-consistent-field ground-state calculation. Effects from small components integrals contribution are neglected.

III. RESULTS AND DISCUSSION

A. Photoelectron spectra of KBr

At first, we compare our calculated results with available experimental data for ionization energies of potassium bromide. The experimental photoelectron spectrum of KBr shown in Fig. 1(a) was published by Caló *et al.*[9] The spectrum was recorded at photon energy of 61.5 eV at beamline I411 in MAX-laboratory, Lund, Sweden. The main structures seen at the ionization energies around 9, 19, 25, 41, and 11 eV were marked with capital letters A, B, C, D, and E, respectively. Our theoretical spectrum in Fig. 1(b) was obtained by convoluting the calculated pole strengths with Gaussian and Lorentzian profiles, 250 meV each. Atomic configurations were assigned to spectral structures, according to main contribution to molecular orbitals (MO).

Comparison between theoretical and experimental ionization energies is summarized in Table I. In the first column singly ionized states are presented according to the leading atomic contribution to the molecular orbital. CI and MCSCF calculations taken from Ref. 9 are shown in the second column.

There are three molecular-field-split $^2\Pi_{3/2}$, $^2\Pi_{1/2}$, and $^2\Sigma_{1/2}$ states in the Br 4p valence region. A Mulliken population analysis yielded a potassium contribution of 2% to $^2\Sigma_{1/2}$

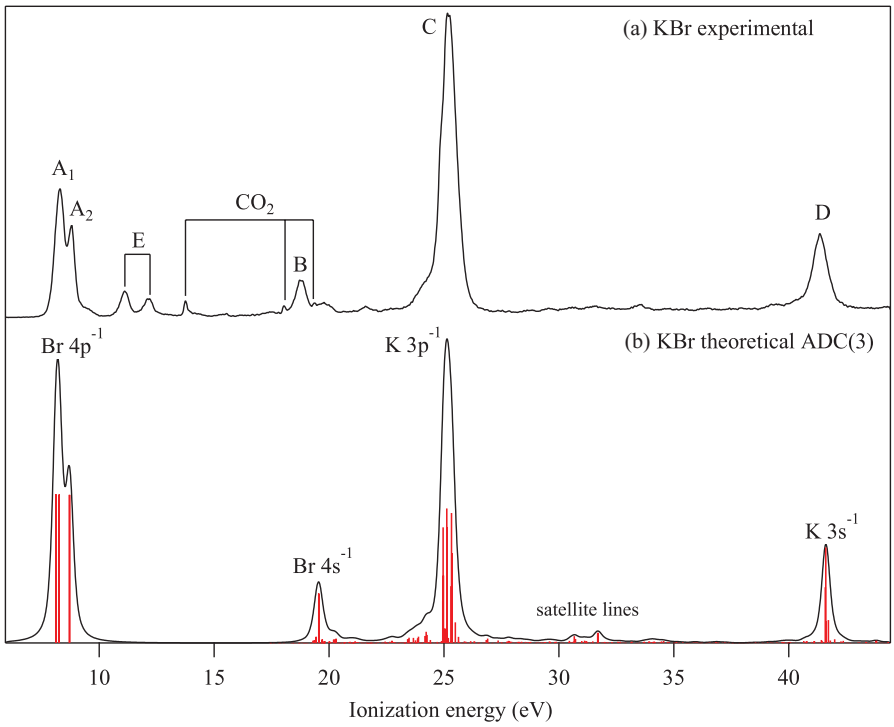

FIG. 1. (a) Experimental valence photoelectron spectrum of KBr molecule measured at 61.5 eV photon energy. (b) The fully relativistic calculated ionization spectrum of KBr molecule at the ADC(3) level convoluted with Lorentzian and Gaussian profiles.

TABLE I. Comparison between experimental energies and theoretical results for singly ionized states taken from the CI, MCSCF, and fully relativistic ADC(3) calculations. All values are given in electronvolts.

	Ionization energy		
Lead. config.	CI/MCSCF	ADC(3)	Expt.[a]
Br $(4p^{-1})$ $^2\Pi_{3/2}$	7.07[b]	8.12	8.29
$^2\Pi_{1/2}$	7.25[b]	8.26	8.29
$^2\Sigma_{1/2}$	7.89[b]	8.71	8.80
Br $(4s^{-1})$	21.90[c]	19.45	18.84
K $(3p^{-1})$	27.26[c]	25.10	25.17
K $(3s^{-1})$	48.18[c]	41.90	41.35

[a]Experimental data from Ref. 9.
[b]CI calculation from Ref. 9.
[c]MCSCF+SO calculation from Ref. 9.

state whereas $^2\Pi_{3/2}$, $^2\Pi_{1/2}$ states were found to exclusively exhibit a bromine character.

The average deviation of ionization energy, obtained by CI method for the first three peaks of the outer-valence region up to 15 eV is around 1 eV in comparison to the experimental value, whereas ADC(3) method reproduced obtained energies within 0.1 eV. $^2\Pi_{3/2}$-$^2\Pi_{1/2}$ splitting of KBr was not resolved experimentally. ADC(3) calculations predicted that the splitting is approximately 0.14 eV (Fig. 1(b)).

The double peak structure at 11.1 eV and 12.1 eV indicated as E in Fig. 1(a) has been identified as Br 3*d* photolines[9] arising from the small second order contribution of the monochromator (123 eV).

In the inner-valence region around 15–30 eV, there are two peaks B and C (see Fig. 1(a)) which originate mainly from Br 4*s* and K 3*p* atomic orbitals, respectively. Ionization energies for B and C peaks predicted by CI and ADC(3) methods deviate from experiment in average by 2.3 eV and 0.3 eV, respectively. Configuration interaction method used by Caló *et al.*[9] fails in reproducing ionization energy for peaks originating from the K 3*s* atomic orbital (peak D in Fig. 1(a)). Ionization energy for that peak deviates by 7.6 eV from the experimental value of 41.35 eV, whereas ADC(3) agrees within 0.6 eV.

In the inner-valence region 20–45 eV we see a dense structure of additional satellites lines. These lines predominantly occur due to coupling of two-hole-one-particle (2h1p) configurations with the initial main one-hole (1h) state. This phenomenon leads to the distribution of the intensity of the main line over several satellite lines. ADC method provides information about electron correlated states, where final cationic state is seen as linear combination of 1h, 2h1p, 3h2p...excited configurations. More discussions about satellites structures can be found in Refs. 9 and 11.

Intensity distribution across the binding energy region is based on occupation of orbitals (statistical weights) in present calculations as actual values of dipole matrix elements are omitted. However, as seen from a comparison between experiment and theory, if energies are well predicted, assignment of all structures becomes possible.

B. Photoelectron spectra of LiBr, NaBr, KBr, and RbBr

ADC(3) calculated ionization spectra of the outer and inner-valence regions of the LiBr, NaBr, KBr, and RbBr molecules are shown in Figs. 2(a)–2(d), respectively. Calculated and experimentally obtained energies for three outermost cationic states of different alkali bromides are compared with available experimental results[6] and collected in Table II. A similar analysis of the electronic structures of alkali iodide monomers was presented in Ref. 11.

The outer-valence electronic structure of alkali bromides, as well as alkali iodides, has identical character and consists of three ligand-field split cationic states, originating from π and σ molecular orbitals with pronounced Br 4*p* character. Inner-valence region includes features which originate from 4*s* orbital of atomic Br and from *p* orbitals of alkali atom. Cross section studies by Price, Potts, and Streets[29] showed that molecular orbitals resulting largely from *p* atomic orbitals have larger HeI photon cross sections than those resulting predominantly from *s* atomic orbitals. Thus, one would expect $\pi_{3/2}$, $\pi_{1/2}$, and $\sigma_{1/2}$ bands with atomic *p* origin to be of the same intensity and shape and to be stronger than σ band of atomic *s* origin. So, we would expect to see similar intensity ratio for the valence peaks of LiBr, NaBr, RbBr than what was measured for KBr (see Fig. 1(a)).

In the valence region 0–15 eV three cationic states with pole strength of 0.94 are clearly visible. The outermost two spin-orbit split $^2\Pi_{3/2}$, $^2\Pi_{1/2}$ states originated mainly from Br atom, whereas $^2\Sigma_{1/2}$ additionally has a small alkali metal contribution. The highest alkali metal contribution to $^2\Sigma_{1/2}$ state, about 11%, was calculated for LiBr, whereas for other alkali halides the metal contribution is less than 2%. Moreover, 2% metal contribution to $^2\Pi_{1/2}$ state was calculated for LiBr. All the outer-valence states are in good agreement with the one-particle picture of the ionization process.

As seen from Table III, for the outermost state $^2\Pi_{3/2}$, the contribution of atomic Br p_x and Br p_y subshells is 98% for all molecules. In contrast, $^2\Pi_{1/2}$ and $^2\Sigma_{1/2}$ states are totally mixed from p_x, p_y, p_z atomic subshells of bromine. Thus, we could assign them to $^2\Pi$ or $^2\Sigma$ states only on the basis of the main atomic contribution to molecular orbital. The p_z contribution to $^2\Pi_{1/2}$ state is increasing in going to heavier metal atom. The reverse situation occurs for $^2\Sigma_{1/2}$ state, where p_z contribution is about 77% for LiBr and decreases to 54% for RbBr. One would expect to find $^2\Sigma_{1/2}$ at lower ionization energy than $^2\Pi_{1/2}$ for CsBr molecule.

In terms of partial ionic character, increased polarization of the halogen atom is related to increased covalent character of the metal–halogen bond.[5] Going from LiBr to RbBr the chemical bond becomes more ionic and less covalent.

While the outer-valence ionization spectra of LiBr, NaBr, KBr, and RbBr have been published before[5,6,9] the inner-valence structures have not been discussed earlier in details. We will first take a look at the main inner-valence peak structures of LiBr, NaBr, and RbBr separately and later on we will follow the tendency of spectral features in general for LiBr to RbBr. Inner shell region of KBr was already discussed above and will only be included when discussing the evolution of the inner-valence features.

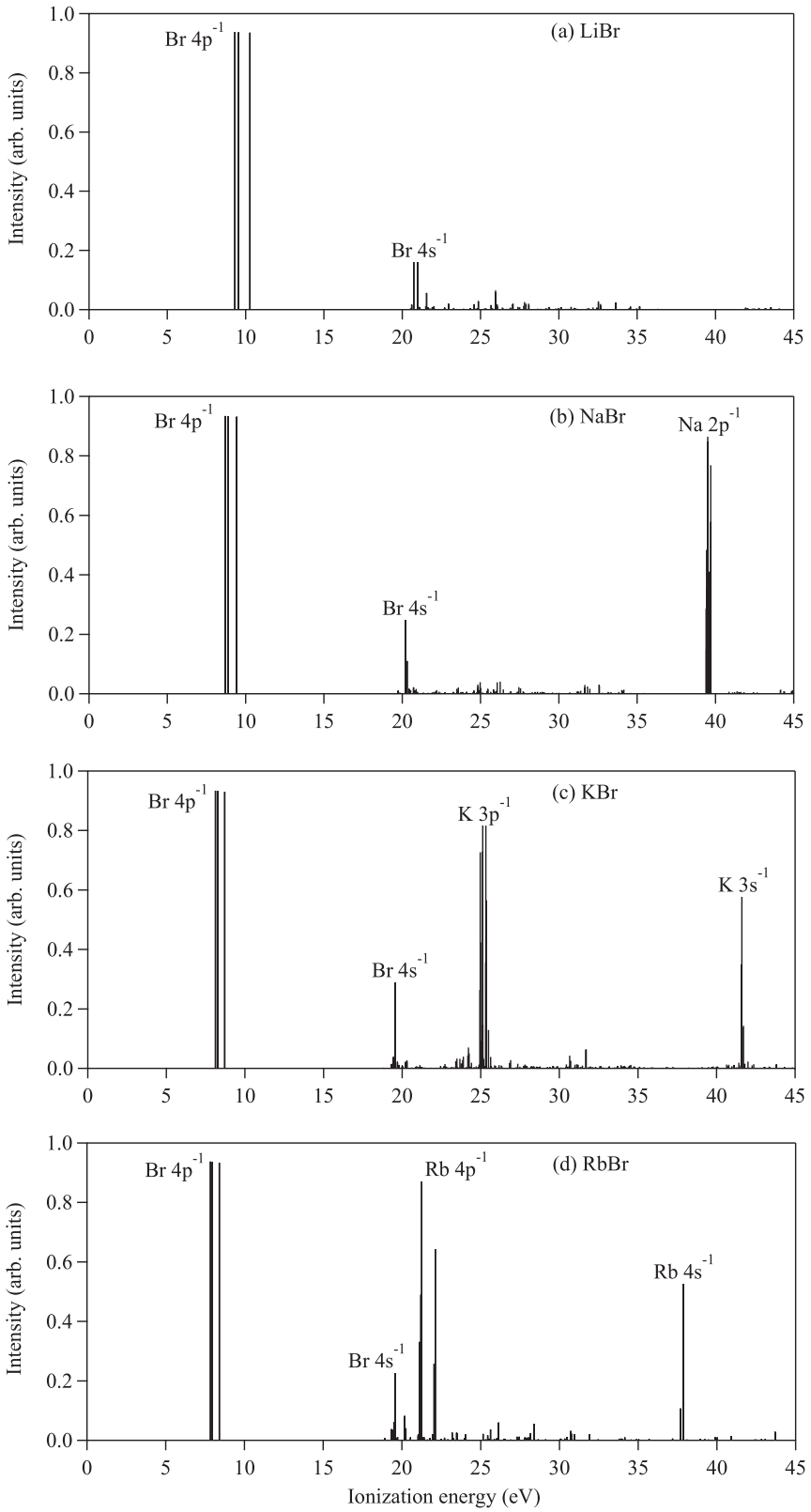

FIG. 2. The fully relativistic calculated ionization spectra of LiBr (a), NaBr (b), KBr (c), and RbBr (d), at the ADC(3) level.

ADC(3) calculations for LiBr predict that one would find a peak, which originates from Br 4*s* atomic orbital, around 20.8 eV (see Fig. 2(a)). Br $4s^{-1}$ peak breaks down to two close lying lines due to many-body interaction. In addition, a dense set of satellite lines accompanies the main Br $4s^{-1}$. The atomic contributions to the Br $4s^{-1}$ peak, according to Mulliken population analysis are 95% of Br 4*s* and 3% of Li 1*s* orbitals.

The calculated spectrum of NaBr (see Fig. 2(b)) shows two peaks lying at around 20.2 eV and 39.5 eV, which

TABLE II. Theoretical ADC(3) and experimental energies (in eV) of three outer valence cationic states of XBr (X = Li, Na, K, Rb) compounds.

	Theoretical			Experimental[a]		
	$^2\Pi_{3/2}$	$^2\Pi_{1/2}$	$^2\Sigma_{1/2}$	$^2\Pi_{3/2}$	$^2\Pi_{1/2}$	$^2\Sigma_{1/2}$
LiBr	9.31	9.55	10.28	10.00	10.60	11.60
NaBr	8.70	8.89	9.43	8.70	9.40	10.30
KBr	8.12	8.26	8.71	8.10	8.60	9.30
RbBr	7.84	7.95	8.39	8.00	8.40	8.80

[a]Reference 6.

correspond to Br 4*s* and Na 2*p* atomic orbitals, respectively. Mulliken population analysis predicts contribution to the Br $4s^{-1}$ peak to be about 99% of Br 4*s* atomic orbital.

The calculated spectrum of RbBr is presented in Fig. 2(d). In the inner-valence region the main structures are seen around 19.6 eV, 21.3 eV, 22.1 eV, and 37.9 eV. They correspond to Br 4*s*, Rb $4p_{3/2}$, Rb $4p_{1/2}$, and Rb 4*s* orbitals, respectively.

Inspection of Fig. 2 shows, that in going from NaBr to RbBr, the np^{-1} peak (n = 2 for Na, 3 for K, and 4 for Rb) approaches the $4p^{-1}$ peak of Br. At the same time, the splitting inside the peaks increases heavily. The peak also overlaps more and more with the satellite peak structure accompanying the Br $4s^{-1}$ peak. Many-body effects clearly play a strong role in the inner-valence region due to near degeneracy of several molecular states.

It is a challenging task to correctly predict the spectral features in case of strong electron correlation. The density and ionization distribution strongly depend on the number of Lanczos iterations and choosing a basis set in ADC(3) calculations. Overall tendency is clear, as one can see, that quite isolated core-valence Na $2p^{-1}$ peak (see Fig. 2(b)) breaks down to several lines. This effect cannot be described in terms of one electron picture. Even more pronounced breakdown of single particle picture happens for KBr and RbBr molecules. The K $3p^{-1}$ and Rb $4p^{-1}$ peaks (see Figs. 2(c) and 2(d), respectively) shift to lower ionization energies, where they heavily overlap with Br $4s^{-1}$ satellite lines. They also affect the position of Br $4s^{-1}$ main line. Near degeneracy of states leads to a mixing which shifts Br $4s^{-1}$ peak towards Br $4p^{-1}$ peaks.

TABLE III. Bromine p_x, p_y, p_z atomic contribution to the first three outer-valence MO-spinors based on Mulliken population analysis at the Dirac-Hartree-Fock (DHF)-level. All values are given in (%). Contributions smaller than 1% and contributions from alkali metal are not included.

	Population					
	$^2\Pi_{3/2}$		$^2\Pi_{1/2}$		$^2\Sigma_{1/2}$	
Molecule	p_x+p_y	p_z	p_x+p_y	p_z	p_x+p_y	p_z
LiBr	98	...	86	10	12	77
NaBr	98	...	76	23	24	74
KBr	98	...	62	36	38	61
RbBr	98	...	56	41	42	54

TABLE IV. Comparison of the spin-orbit splittings of Na, K, and Rb np^{-1} ($n = 2, 3, 4$) peaks in XBr (X = Na, K, Rb) molecules with atomic spin-orbit splittings.

	Na $2p^{-1}$	K $3p^{-1}$	Rb $4p^{-1}$
Molecule	0.26	0.36	0.86
Atom[30]	0.27	0.36	0.69

Next, we will compare calculated ADC(3) spin-orbit splittings of Na, K, and Rb np^{-1} ($n = 2, 3, 4$) levels in XBr (X = Na, K, Rb) molecules with pure atomic spin-orbit splittings.[30] An atomic configuration $np^5(n+1)s$ gives rise to 4 states due to coupling of *np* hole with $(n+1)s$ valence electron. In order to estimate atomic spin-orbit splitting we averaged energies of the states corresponding to $np_{1/2}$ and $np_{3/2}$ holes. As one can see from Fig. 2, calculated Na $2p^{-1}$ and K $3p^{-1}$ peaks do not have clear spin-orbit splittings and therefore the widths of the corresponding group of lines were taken as estimations. Instead, Rb $4p^{-1}$ peak has clearly visible spin-orbit splitting. The results are summarized in Table IV.

As seen from Table IV, the spin-orbit splitting of Na $2p^{-1}$ and K $3p^{-1}$ peaks is directly comparable with atomic spin-orbit splitting, while Rb $4p^{-1}$ spin-orbit splitting is most probably effected by contribution from Br $4s^{-1}$ satellites. Overall correct reproduction of the inner-valence spectral features requires an adequate treatment of relativity and electron correlation.

IV. CONCLUSIONS

We have studied the valence photoelectron spectra of alkali bromides XBr (X = Li, Na, K, Rb) within the framework of the propagator theory. The ADC(3) method is shown to be an effective tool in calculation of the inner-valence region for molecules where heavy elements are presented. The theoretically calculated valence ionization spectrum of potassium bromide is in good agreement with experiment.

ADC(3) theoretical calculations of the valence ionization spectra of LiBr, NaBr, and RbBr molecules were presented in this work for the first time and should have predictive character for future experimental investigation.

Discrepancy between the theoretical and experimental relative intensity might exist due to the fact that ADC(3) method does not take into account dipole matrix elements between bound one-particle state and the continuum state.

ACKNOWLEDGMENTS

This work has been supported by the Research Council for the Natural Sciences and Engineering of the Academy of Finland.

[1]J. Berkowitz, C. H. Batson, and G. L. Goodman, J. Chem. Phys. **71**, 2624 (1979).
[2]A. W. Potts and E. P. F. Lee, J. Chem. Soc., Faraday Trans. 2 **75**, 941 (1979).
[3]J. Niskanen, S. Urpelainen, S. Aksela, H. Aksela, O. Vahtras, V. Carravetta, and H. Ågren, Phys. Rev. A **81**, 043401 (2010).
[4]R. T. Poole, R. C. G. Leckey, J. G. Jenkin, and J. Liesegang, Chem. Phys. Lett. **31**, 308 (1975).

[5]A. W. Potts, T. A. Williams, and W. C. Price, Proc. R. Soc. London, Ser. A **341**, 147–161 (1974).
[6]T. D. Goodman, J. D. Allen, Jr., L. C. Cusachs, and G. K. Schweitzer, J. Electron Spectrosc. Relat. Phenom. **3**, 289–304 (1974).
[7]M. Patanen, J. Niskanen, M. Huttula, K. Jänkälä, S. Urpelainen, H. Aksela, and S. Aksela, J. Phys. B **41**, 215103 (2008).
[8]E. Kukk, M. Huttula, H. Aksela, S. Aksela, E. Nömmiste, and A. Kikas, J. Phys. B: At. Mol. Opt. Phys. **36**, L85 (2003).
[9]A. Caló, M. Huttula, M. Patanen, H. Aksela, and S. Aksela, J. Electron Spectrosc. Relat. Phenom. **162**, 30 (2008).
[10]P. Tomasello and W. von Niessen, Europhys. Lett. **7**, 405 (1988)
[11]M. Pernpointner and S. Knecht, Chem. Phys. Lett. **410**, 423 (2005).
[12]M. Pernpointner, S. Knecht, and L. Cederbaum, J. Chem. Phys. **125**, 034309 (2006).
[13]W. von Niessen, J. Schirmer, and L. S. Cederbaum, Comput. Phys. Rep. **1**, 57–125 (1984).
[14]L. S. Cederbaum and W. Domke, Adv. Chem. Phys. **36**, 205–344 (1977).
[15]J. Schirmer, L. S. Cederbaum, and O. Walter, Phys. Rev. A **28**, 1237 (1983).
[16]D. Danovich, Wiley Interdiscip. Rev.: Comput. Mol. Sci. **1**, 377–387 (2011).
[17]F. Tarantelli and L. S. Cederbaum, Phys. Rev. A **39**, 1639 (1989).
[18]F. Tarantelli and L. S. Cederbaum, Phys. Rev. A **39**, 1656 (1989).
[19]M. Pernpointner, J. Chem. Phys. **121**, 8782 (2004).
[20]M. Pernpointner, J. Phys. B **43**, 205102 (2010).
[21]T. Saue, L. Visscher, and H. J. Aa. Jensen, with contributions from R. Bast, K. G. Dyall, U. Ekström, E. Eliav, T. Enevoldsen, T. Fleig, A. S. P. Gomes, J. Henriksson, M. Iliaš, Ch. R. Jacob, S. Knecht, H. S. Nataraj, P. Norman, J. Olsen, M. Pernpointner, K. Ruud, B. Schimmelpfennig, J. Sikkema, A. Thorvaldsen, J. Thyssen, S. Villaume, and S. Yamamoto, DIRAC, a relativistic *ab initio* electronic structure program, Release DIRAC10, 2010, see http://dirac.chem.vu.nl.
[22]A. Honig, M. Mandel, M. L. Stitch, and C. H. Townes, Phys. Rev. **96**, 629 (1954).
[23]F. J. Lovas and E. Tiemann, J. Phys. Chem. Ref. Data **3**, 609 (1974).
[24]G. M. Rothberg, J. Chem. Phys. **34**, 2069 (1961).
[25]R. Krishnan, J. S. Binkley, R. Seeger, and J. A. Pople, J. Chem. Phys. **72**, 650 (1980).
[26]A. D. McLean and G. S. Chandler, J. Chem. Phys. **72**, 5639 (1980).
[27]J.-P. Blaudeau, M. P. McGrath, L. A. Curtiss, and L. Radom, J. Chem. Phys. **107**, 5016 (1997).
[28]K. G. Dyall, Theor. Chem. Acc. **115**, 441 (2006); see http://dirac.chem.sdu.dk for basis sets available from the DIRAC web site.
[29]W. C. Price, A. W. Potts, and D. G. Streets, *Electron Spectroscopy*, edited by D. A. Shirley (North-Holland Publ. Co., Amsterdam, 1972), pp. 187–198.
[30]NIST Atomic Spectra Database, version 5.0, see http://physics.nist.gov/asd.